Materials Science & Engineering A 573 (2013) 45–53

Contents lists available at SciVerse ScienceDirect

Materials Science & Engineering A

journal homepage: www.elsevier.com/locate/msea

Influence of the crystalline orientations on microcrack initiation in low-cycle fatigue

P. Mu [a,b,e], V. Aubin [c,e,*], I. Alvarez-Armas [d], A. Armas [d]

[a] Univ Lille Nord de France, F-59000 Lille, France
[b] ECLille, LML, F-59650 Villeneuve d'Ascq, France
[c] ECP, MSSMat, F-92295 Châtenay-Malabry, France
[d] IFIR, CONICET, Universidad Nacional de Rosario, Argentina
[e] CNRS, UMR 8107, UMR 8579, France

ARTICLE INFO

Article history:
Received 9 July 2012
Received in revised form
18 February 2013
Accepted 21 February 2013
Available online 27 February 2013

Keywords:
Low-cycle fatigue
Austenitic stainless steel
In situ observation
EBSD
Crack initiation
Crystalline orientation

ABSTRACT

Present study aims at analyzing the crack initiation in an austenitic stainless steel in low-cycle fatigue. A fatigue test was carried out using a polished specimen. The surface of the specimen was observed in situ during the fatigue test, in order to establish the time of slip activity or crack initiation. After a number of cycles sufficient to initiate small cracks, the test was stopped and the surface observed by scanning electron microscopy. The electron backscattered diffraction technique (EBSD) was used to identify the orientations of surface grains in the central zone of the fatigue specimen. Crack-initiation sites and slip systems associated to the initiated microcracks were identified. The criterion of the maximum Schmid factor explains two-thirds of the cracks initiated in slip systems; however if the favorably oriented slip band with respect to this criterion makes an angle of around 45° to the loading direction, a crack may initiate in another slip system.

1. Introduction

Austenitic stainless steels combine good mechanical properties to an excellent corrosion resistance. This combination made austenitic stainless steels the most widely used type of stainless steels. In structural applications, they are subjected to cyclic loadings, which may induce the initiation of several cracks and their propagation. In 316L stainless steel, during fatigue, plastic strain irreversibility is localized in dislocation structures in the patterns of sheets, imperfect vein structure with persistent slip bands or in cells and wall structures. The dislocation pattern in the material depends mainly on plastic strain amplitude, temperature and nitrogen content, etc. [1,2], and can change from low density patterns to high density ones with the increasing number of cycles [3,4]. For 316L stainless steel not alloyed with nitrogen, PSM's profile in individual cross-sections [5] and its cumulative evolution on two mutually perpendicular surfaces [6] have been observed. The use of FIB technique allows to observe the microstructure beneath the surface in relation with the PSM profiles, as it was recently reported in AISI 316L by Man et al. [7]. ECCI observations confirmed that the ladder-like persistent slip bands in the bulk fit perfectly well with the extrusions observed at the surface. These studies showed that plastic straining within PSBs leads to the growth of extrusions which may be accompanied, somewhere only locally, by intrusions. Cracks initiate from the root of deep intrusions, generally from the middle of the grain. They initially propagate along the PSB–matrix interface and can later deviate from the crystalline slip plane [7]. Besides PSBs, plastic strain irreversibility is also localized in grain boundaries (GBs) or twin boundaries (TBs), especially at lower strain amplitudes [8,9]. Cracks initiate in these high loaded zones and, then, slowly propagate.

316L stainless steel alloyed with nitrogen was studied together with the austenitic phase of duplex stainless as the addition of nitrogen induces the same properties [2,10–12]. It is now well known that the addition of nitrogen modifies the dislocation structure observed and promotes planar slip [12]. At the same strain amplitude, when a 316L stainless steel shows cellular arrangement of tangles, only planar slip is visible in 316L stainless steel alloyed with nitrogen [13]. As the plastic strain localization decreases with increasing nitrogen content, a beneficial effect of nitrogen alloying is observed on the fatigue life [12].

The studies presented above provide very precise data obtained in a limited number of cases as FIB or AFM provide only local information. Persistent slip marking can show a high

* Corresponding author at: ECP, MSSMat, F-92295 Châtenay-Malabry, France. Tel.: +33 1 41 13 15 20; fax: +33 1 41 1314 42.
E-mail address: veronique.aubin@ecp.fr (V. Aubin).

0921-5093/$ - see front matter © 2013 Elsevier B.V. All rights reserved.
http://dx.doi.org/10.1016/j.msea.2013.02.046

variability even in a same grain, and this variability can change with the cycling [5]. Together with these local studies, there is a need of statistical approach in the analysis of the fatigue crack initiation domain in order to establish low-cycle fatigue criteria based on microstructural parameters as texture, grain size, grain shape, etc. The present study aims at analyzing the interaction between crack initiation and microstructure in an austenitic stainless steel in low-cycle fatigue. A specific device was used to observe the surface of the specimen in situ during the fatigue test. Electron backscatter diffraction allowed to establish grain orientation of the surface zone analyzed. The sites for crack initiation have been identified, and the orientations of slip systems associated with microcracks have then been analyzed.

2. Material and specimen preparation

The material studied in this work is an AISI 316L austenitic stainless steel. Its chemical composition is given in Table 1. The material was supplied as a rolled plate of 14 mm in thickness. It was solution treated for 1 h at 1050 °C and then water quenched. All alloying elements were, thus, put into solid solution. The studied material has an average grain size of approximately 50 μm (Fig. 1). Twins are commonly observed in the grains.

Table 1
Composition of the AISI 316L stainless steel used in this study (wt%).

C	Cr	Ni	Mo	Mn	Si	P	Fe
≤ 0.030	18.51	12.85	2.15	1.50	0.71	≤ 0.045	64.30

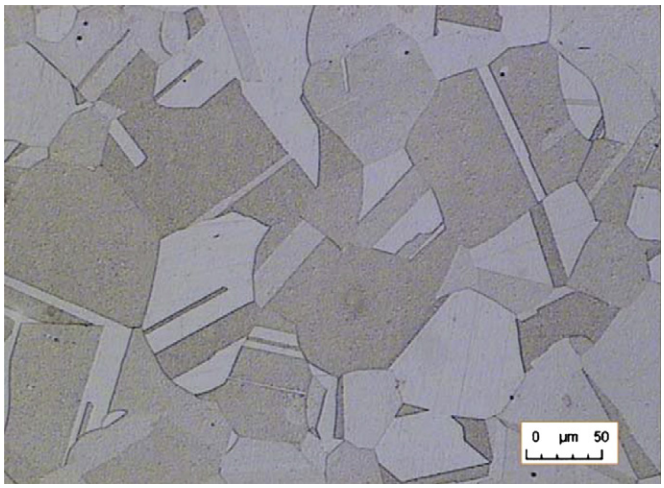

Fig. 1. Microstructure of AISI 316L austenitic stainless steel observed after chemical etching.

3. Experimental procedure

3.1. Low-cycle fatigue test

In order to analyze crack initiation during low-cycle fatigue, a fatigue test was carried out on an electromechanical tension–compression testing machine (Fig. 2). A plate specimen was machined from the as-received sheet. The specimen had a useful rectangular part of 23.72 mm in length, 6 mm in width, and 3.6 mm in depth. The gauge length of the specimen was 10 mm. It was mechanically polished down to 1 μm grade diamond paste. In order to reveal grain boundaries, the specimen was etched in a solution composed of 3 vol. HCl and 1 vol. HNO_3 for 40 s at room temperature. The time for chemical etching should be carefully controlled so that the grain boundaries or twin boundaries were not too much attacked, since they may be preferential crack initiation sites.

The test was controlled in longitudinal strain measured by an extensometer with a gauge length of 20 mm. The cyclic test was carried out under total strain control with a strain rate of $6.6 \times 10^{-4}\,s^{-1}$, a strain amplitude of 0.5% and zero mean strain. This loading corresponds to the plastic strain amplitude of approximately 0.35% (see Fig. 3). Load and strain were simultaneously recorded during the cycling. The specimen was loaded/unloaded until 2000 cycles. The test was paused after every 100 cycles (200 cycles after 1400 cycles) in order to record the damage in the surface of the specimen. As it has been shown by Lindstedt et al. [14] under the same strain amplitude, the crack density in austenitic stainless steels increases until about 1500 cycles and stabilizes. Observations after 2000 cycles allow then to highlight all the crack nucleation sites.

The cyclic hardening/softening curve obtained during the test is shown in Fig. 3. It has been verified that the stress relaxations occurring at each test interruption to take pictures of the specimen surface have no influence on the macroscopic behavior. The experimental mechanical behavior is thus consistent with previous studies carried out on the same material. The material firstly shows a cyclic hardening during the first cycles and then softens until almost

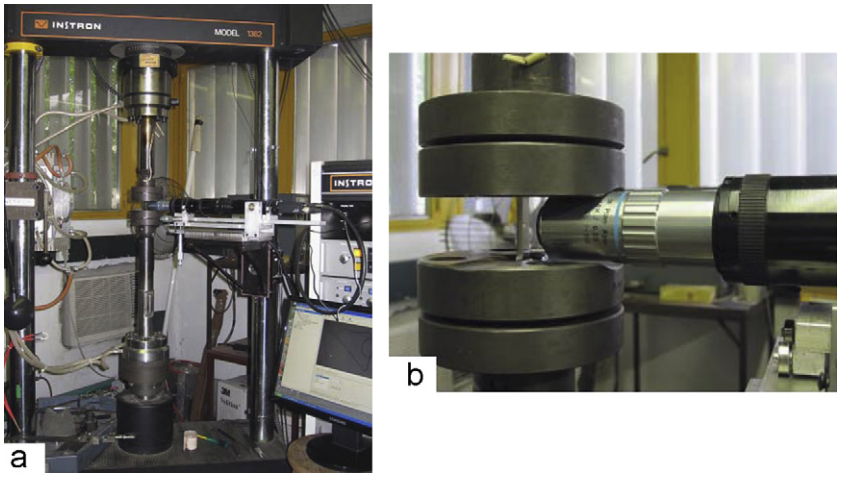

Fig. 2. (a) Experimental equipment and (b) specimen mounted in the grips together with the objective of the camera.

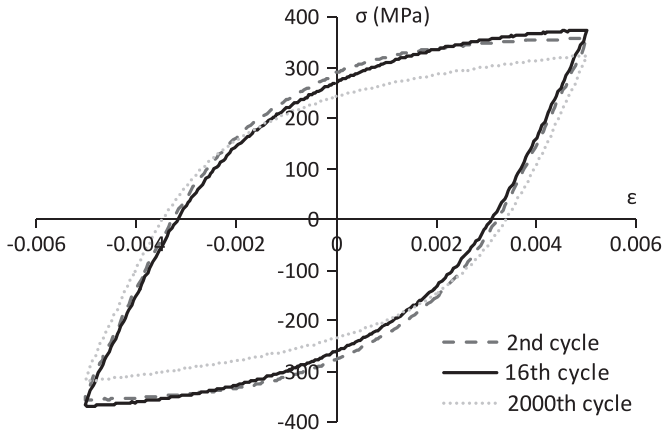

Fig. 3. Hysteresis loops during the hardening stage (2nd cycle), at σ_{max} (16th cycle) and at the end of the softening stage (2000th cycle).

stabilization. In AISI 316L, at room temperature, the stabilization stage covers generally the main part of the fatigue life [15–17]. During the hardening/softening stage, cracks appear at the surface of the specimen. However, these cracks have a depth limited to a few microns, and cannot modify the stiffness of the specimen. During the fatigue life, Young modulus remains almost constant until a predominant crack propagates over a large part of the specimen section [18].

3.2. Observation of the specimen surface

In order to follow the surface damage evolution during the low-cycle fatigue test in real time and to record images at the microstructural scale, and in situ microscopy device was used [19,20]. This device consists of a 10-bit charge-coupled device (CCD) camera (1040 × 518 pixels) equipped with a coaxial objective and a zoom allow to observe a zone of 140 μm × 70 μm (see Fig. 2). This zone was small enough to reveal the fatigue damage at a microstructural scale, and large enough to observe several grains in one image. This zone also ensured an acceptable quality of the images acquired, as the lighting is relatively homogeneous. The in situ observation device was mounted on the frame of the testing machine (Fig. 2a). Two displacement tables permitted to move the camera on a plane parallel to the studied specimen surface. The working distance of the camera was 13 mm and the depth of field was about 1 μm.

A domain of 8 × 6 (horizontal no. × vertical no.) images was observed during the test. The total dimensions of the observation domain were 1080 μm × 400 μm. Images of this domain were first acquired before the test. Then, during the test, the cycling was interrupted every 100 cycles and 8 × 6 images were taken. After 2000 cycles, the test was stopped and the same domain was observed in SEM. Every image of a given zone was taken carefully in order to represent exactly the same zone of the specimen, which enables to observe the fatigue damage changes at the specimen surface directly. Observations in this study were done in a scanning electron microscope HITACHI S3600, mainly on secondary electrons, with an accelerating voltage of 15 kV.

The optical observation zone was limited (1.08 mm × 0.4 mm), only three cracks initiated in this zone. In order to have enough cracks for a statistical analysis, two bigger zones (2.1 mm × 2.0 mm) were observed in SEM, the first one including the optical observation zone. 4 micro-indentations were made at the surface of specimen to precisely localize optical and SEM zones.

EBSD measurements were performed on the specimen surface after the mechanical test to obtain crystallographic orientations of surface grains and the grain boundary arrangement. EBSD scans were performed in beam control mode with a spatial resolution of 4 μm/step. The two zones (2.1 mm × 2.0 mm) observed in SEM were scanned, they contained about 12,000 grains.

4. Surface plastic activity and crystallographic analysis on crack orientation

4.1. Analysis of the plastic activity

A domain of 1080 μm × 400 μm was followed during the test using the in situ microscopy device. Images of a same zone obtained before the test, after 500 cycles, and after 2000 cycles are shown in Fig. 4. Surface changes during the cyclic test in a given observation zone can be seen in this figure. Before the test, only grain boundaries and twin boundaries could be seen. After 500 cycles, several slip lines appeared in some grains. After 2000 cycles, slip bands intensified and could be seen in almost all grains. In some grains, several slip systems were activated.

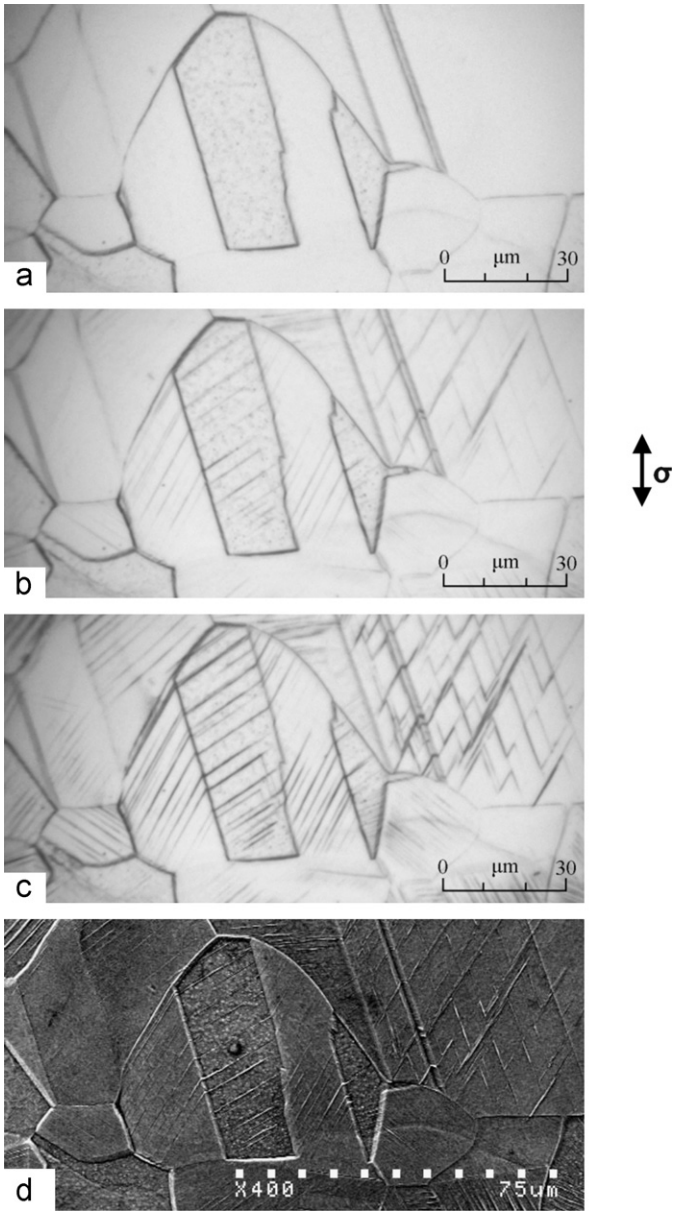

Fig. 4. Images of the same zone taken first optically (a) before the test, (b) after 500 cycles, (c) after 2000 cycles and (d) with a SEM after 2000 cycles.

The analysis of these images allows characterization of the plastic activity during the cycling. At various numbers of cycles, the number of grains showing slip markings was counted. About two-thirds of the grains showed plastic activity after 300 cycles, they were about 90% after 2000 cycles.

In order to distinguish cracks from slip markings and to measure the orientations of slip bands and cracks, the zone shown in Fig. 4a–c has been observed in SEM after the test (Fig. 4d). Slip systems activated have been identified in each grain of the observed zone following the procedure detailed in [21]. From Euler angles measured, for each potential slip system (12 systems), the Schmid factor μ and the angle Π between the possible slip markings appearing at the free surface and the loading axis were calculated. A slip system is supposed to be activated when associated slip markings are observed at the surface. For each slip marking, the experimentally measured angle Π was compared to those calculated above. The slip plane with the closest angle Π to the measured value of Π was considered activated. The slip direction is determined making the assumption that the activated slip system is that with the highest Schmid factor among the three possible slip systems.

In most grains, only 1 or 2 slip systems are activated. The activated slip system usually has the highest Schmid factor, except in some rare cases. It is important to note that the grains in a polycrystal are in a triaxial state and their deformations are also influenced by the deformations of neighbor grains. This may explain the activation of a slip system of which the Schmid factor is not the highest.

Fig. 5 shows the cumulative frequency of the highest Schmid factors of all grains in the analyzed zone. It can be seen that for the grains of the analyzed zone, the highest Schmid factor is always higher than 0.30. This distribution was compared with the highest Schmid factors of the activated slip systems in 178 grains showing plastic activity. The two distributions are globally in good agreement confirming the validity of the criterion of the highest Schmid factor for slip system activation. The agreement is poorer for Schmid factors in the range [0.35, 0.41].

Some grains of the analyzed zone present multiple slip. The Schmid factors of the activated slip systems have been specifically analyzed (Fig. 6a). It can be seen that the range, where the highest Schmid factor is higher than 0.45 and where the second is higher than 0.4, represents more than 60% of the grains with multiple slips. Grains showing multiple slip are mainly oriented for double slip. The two activated slip systems activate one after the other. In Fig. 4, the slip markings are straight and fine, and parallel to each other. These characteristics are typical of planar slip. Austenitic stainless steels 316L have low stacking fault energy (SFE), which

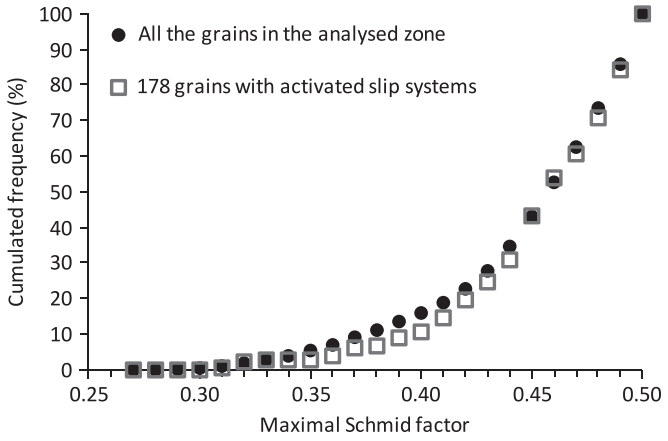

Fig. 5. Cumulative frequencies of the maximal Schmid factors of the grains of the analyzed zone and of activated slip systems in 178 analyzed grains.

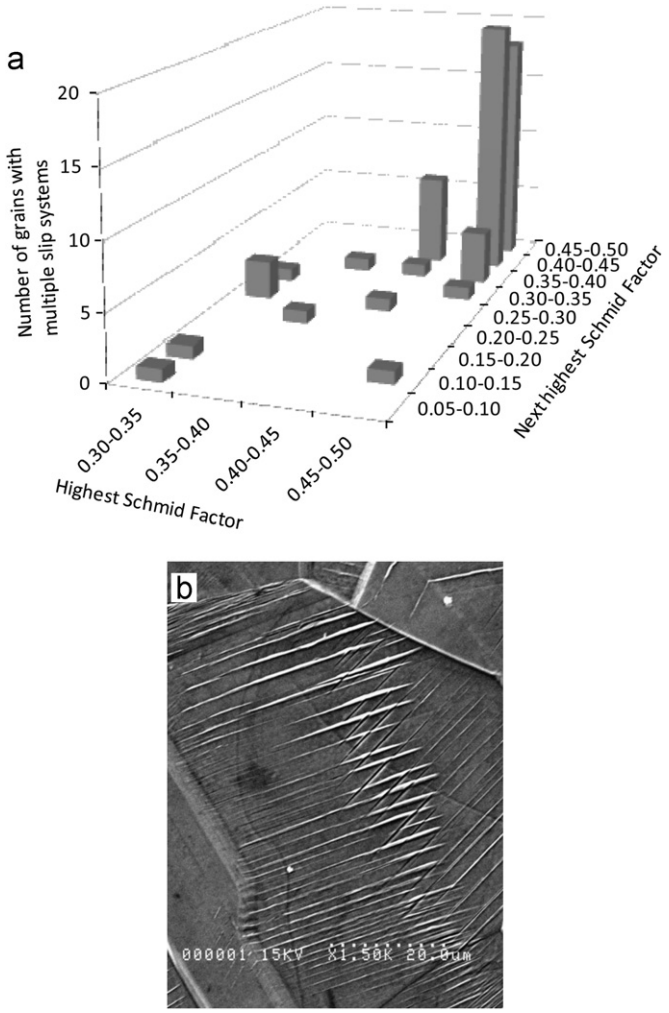

Fig. 6. (a) Distribution of highest and next highest Schmid factors in grains showing multiple slip systems activated and (b) a grain with two activated slip systems observed in SEM.

favors planar slip. The stacking fault energy strongly depends on the nitrogen content and varies from 25 ± 5 mJ/m^2 in AISI 316L with low nitrogen content [2,22] down to about 10 mJ/m^2 in AISI 316L with 0.22% of nitrogen [24]. The additional N reduces the tendency to cross slip and favors planar slip [2,10–13,16]. In a 316LN stainless steel, at total strain amplitude of 0.5%, identical to the loading applied in the study presented here, dislocation structures observed at half fatigue life are predominantly planar structures [23]. Veins and PSB are observed in low quantity, and cells develop only in the vicinity of grain boundaries [23], whereas 316L stainless steels show veins, PSB, cells and labyrinths. This effect of nitrogen alloying may not be only due to the decrease in SFE but also to the strong affinity between nitrogen and chromium, which increases short range order in this family of alloys [24,25]. Moreover, it was also shown that a higher nitrogen content decreases the crack propagation rate compared to austenitic stainless steel alloyed with a lower N content [13]. The lower crack propagation rate was explained by the more difficult cross slip in 316LN compared to 316L at the same strain amplitude [2].

Although the content in nitrogen of the studied alloy is not known, these observations indicate that it should be relatively high. Moreover, the fact that several slip systems with very high Schmid factors activate confirms this assumption. As the cross-slip is not easy, in certain grains, two slip systems are activated to accommodate the plastic deformation.

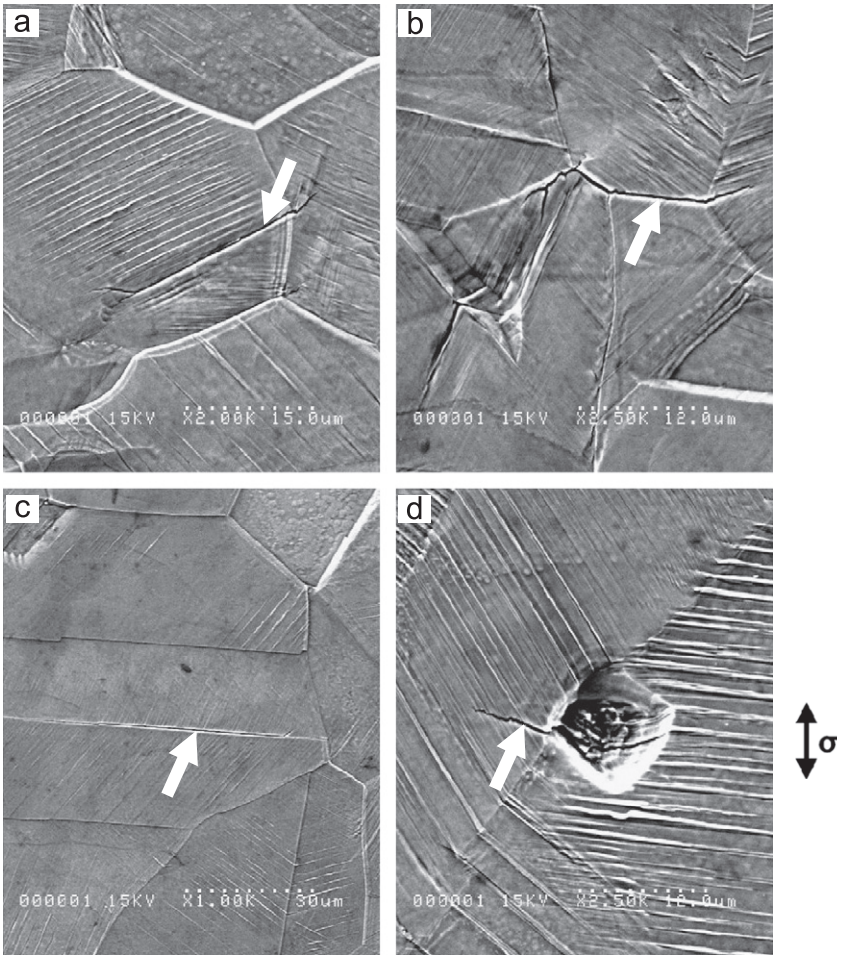

Fig. 7. Cracks initiated in a slip band (a), at a grain boundary (b), at a twin boundary (c), and from an inclusion (d). Cracks are indicated by arrows.

4.2. Crack orientation analysis

All the cracks in the SEM observation zone (8.4 mm^2) were looked for and analyzed. The crack density after 2000 cycles was 30 cracks/mm^2. It depends on the loading conditions (strain amplitude, environment) [26,27] and on the material (grain size, nitrogen content) [14]. Four crack initiation origins were found: cracks initiate in slip bands (SB) (Fig. 7a), at grain boundaries (GB) (Fig. 7b), at twin boundaries (TB) (Fig. 7c), or from inclusions (Fig. 7d). Only very few cracks were initiated from inclusions (about 1%). The distributions of SB, GB and TB cracks have been determined. When the type of a given crack was uncertain between two classes, it counted for half in each class. It can be seen that, at room temperature, under a medium strain amplitude ($\varepsilon_a = 5 \times 10^{-3}$, $\varepsilon_a^p \approx 3.3 \times 10^{-3}$) after 2000 cycles, cracks appear mainly in slip bands (51%) and in grain boundaries (44%). Cracks initiated in twin boundaries (5%) occupy only a very little proportion. These results can be compared to those of Mineur et al. [26] and Kamaya [28], both obtained in cyclically strained type AISI 316 austenitic stainless steels under various strain amplitudes. In the literature, it is observed that the highest the strain amplitude, the less cracks initiate in slip bands, which is consistent with observations showing that in the high cycle fatigue domain cracks initiate preferentially in slip bands [29].

Fig. 8 shows the cumulated frequency of the maximal Schmid factor, on one hand, in all the grains in the studied zone, and, on the other hand, in the 91 grains showing SB cracks. It can be seen that no crack initiated in a grain with a maximal Schmid factor less than 0.40. All the grains showing cracks are then oriented for single slip. The cumulated frequency of maximal Schmid factor in grains showing SB cracks is much lower than that obtained in all grains, there are many grains showing cracks with a very high maximal Schmid factor. This means that crack initiation is much easier in grains with very high maximal Schmid factors.

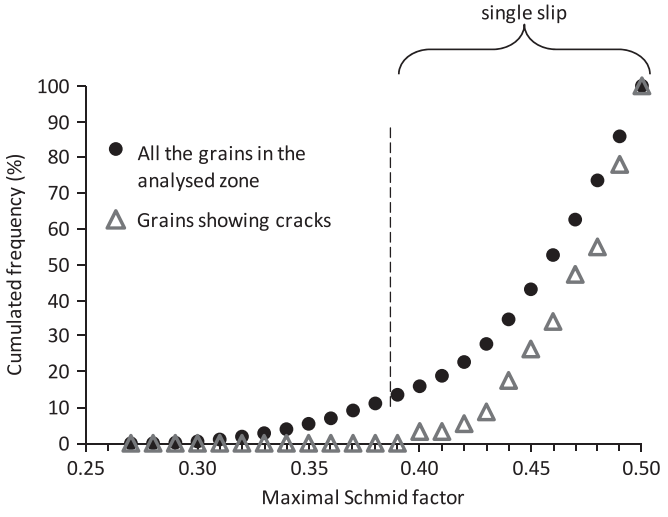

Fig. 8. Cumulated frequency of maximal Schmid factors of, in the one hand, all the grains, and, in the other hand, the grains showing SB cracks.

Fig. 9 shows the cumulated Schmid factors of the slips systems associated with the crack in grains showing SB cracks, considering

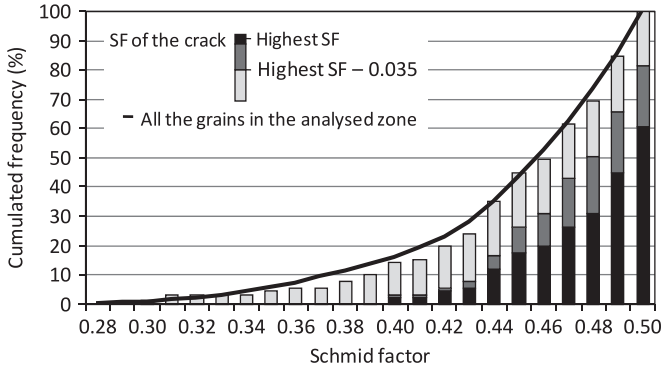

Fig. 9. Cumulated maximum SF in all the grains and SF associated with the cracked slip system in grains showing SB cracks. Grains have been divided into three groups, depending on the difference between the highest Schmid factor of the grain and their SF.

three groups of cracks, depending on the difference between the highest Schmid factor of the grain and the Schmid factor related to the cracked slip system. Most of the cracks (64%) initiated on the slip system with the highest Schmid factor (SF_{max}), 18% of the cracks have a Schmid factor close to the maximum Schmid factor, and 19% of the cracks have a Schmid factor lower than $SF_{max}-0.035$. Fig. 13 shows that cracks having the maximum Schmid factor (1st group) have SF mainly in the range [0.44, 0.50]. For the 2nd group, Schmid factors associated with cracked slip systems are mainly in the range [0.44, 0.48] and for the 3rd group, in the range [0.30, 0.44]. Fig. 9 also compares the Schmid factors associated with cracked slip systems for the grains showing SB cracks to the maximal Schmid factors of all grains in the studied zone. The two curves are in good agreement, contrary to Fig. 8. This shows that in many grains, the slip system which leads to crack initiation is not the slip system with the maximal Schmid factor. The Schmid factor is thus not the only criterion to be considered to explain crack initiation.

Fig. 10 shows the distribution of crack orientations for those initiated in slip bands. The angle Π between the load axis and each crack was measured (Fig. 10a). When a grain contained two cracks with various orientations, both were measured and the Schmid factors corresponding to the associated slip systems were calculated. Only the crack with the highest Schmid factor is considered here. The crack orientation distribution is plotted in Fig. 10b with respect to the Schmid factor of the slip system associated with the crack. Grains have been divided into three groups, depending on the difference between the highest Schmid factor of the grain and the Schmid factor related to the cracked slip system. It can be seen in Fig. 10b that almost no crack initiated in the domain $\Pi \in [0°, 40°]$. A near-symmetrical triangular distribution can be observed, centered in the range [60°–70°], which represents about 25% of the cracks initiated in slip bands. Considering the link between angle Π and the Schmid factor of the associated slip system, it is observed that cracks with low Schmid factors (3rd group) are not distributed equally but have angle Π belonging to [60°, 90°] only.

The distribution of crack orientations is also compared in Fig. 10b to the orientations of the potential traces at the surface of the slip systems having the highest Schmid factor in all the grains of the analyzed zone. This second distribution is triangular, centered in the range [40°–50°]. Comparing the two distributions, the one for cracks and the second for all grains, it is clear that cracks do not appear randomly in the slip system with the higher Schmid factor. Among all the grains, the slip systems where cracks will preferably initiate make a large angle Π to the loading direction, preferably higher than 60°. On the contrary, cracks making an angle Π smaller than 50° are under-represented.

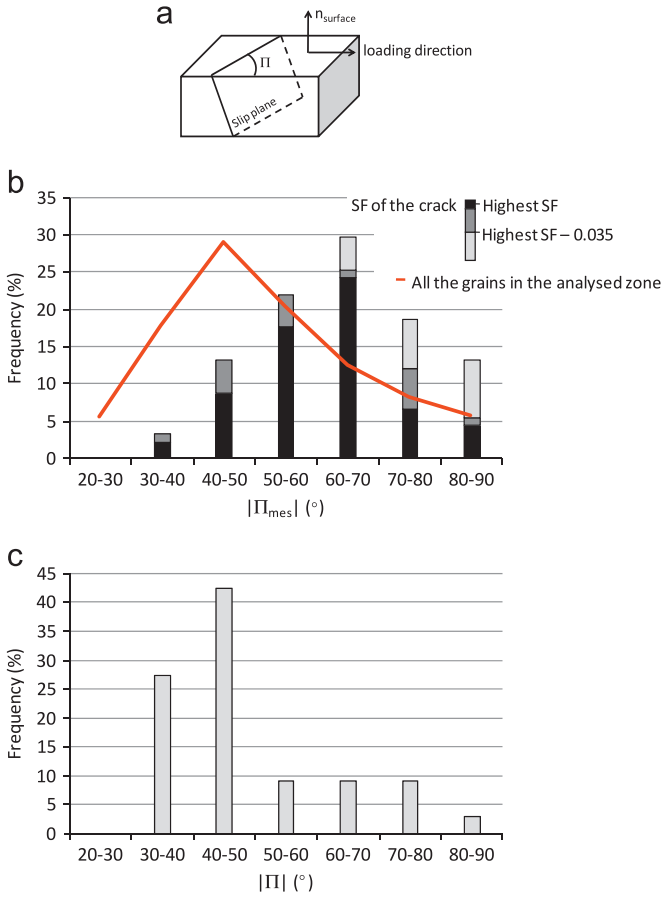

Fig. 10. (a) Angle between the intersection of the slip plane and the surface toward the loading axis, Π; (b) crack orientation distribution (for cracks initiated in slip bands) together with the orientation of potential trace at the surface of the slip system having the highest SF in all the grains of the analyzed zone. Cracks have been divided into three groups, depending on the ratio between the highest SF of the grain and SF of the crack, (c) distribution of angles Π of the slip systems having the highest Schmid factor but not turned into cracks.

Crack orientation can also be analyzed in terms of fracture mechanics. In case of tension-compression loading, it is clear that a crack making an angle Π of 90° on the surface with the direction of loading favours mode I of crack opening, whereas an angle Π of 45° will favor a mixed mode I+II. The fact that mode I is the most damaging is consistent with the observations made in Fig. 10b. It must be noted that the loading mode depends on the location of the point on the crack front and will change from one point to another one, especially if the crack front is not regular. Some recent papers analyzed three-dimensional short fatigue crack growth using FIB or microtomography and showed the crack surface is not plane, even in the first grain [7,9,30]. Crack may branch [7] or deviate from the primary slip plane [7,9,30]. Moreover, the crack growth behavior is complex, as the crack growth rate is not constant along the crack front, which induces an irregular crack front, particularly after crossing the first grain boundaries [31]. A general analysis of crack modes leading to the crack growth in the depth is then difficult, as it needs a 3D analysis of the shape of each crack, together with the crystalline orientation and shapes of the grains surrounding the crack, in order to evaluate the stress field around the crack analyzed.

As in the range [60°, 90°], cracks initiated in another slip system that the best oriented are over-represented, these specific cracks were analyzed carefully. Fig. 10c shows the distribution of angles Π of slip systems with the highest Schmid factor in grains showing SB crack in another slip system. It can be seen that slip

systems with the highest Schmid factor showing no crack are not distributed homogeneously and they are much more numerous in the range of Π belonging to [30°, 50°]. In other words, if the slip system with the maximum Schmid factor makes an angle of Π near or less than 45° to the loading direction, it will probably not form a crack, which will appear on a different slip system. On the other hand, if it makes an angle Π higher than 45°, a crack may likely initiate in this slip system. These observations agree with the classification introduced by Brown and Miller [32]. Among favorable oriented slip systems for simple glide, it was shown that two slip systems have a particular orientation toward the surface: systems A and B. In both cases, slip planes make an angle of 45° to the direction of loading, but the slip direction changes. For system A, the slip direction is parallel to the free surface, and no intrusion–extrusion is created during gliding. On the contrary, for system B, the slip direction makes an angle of 45° to the free surface, and the gliding along this slip system will create roughness at the free surface, where microcracks can initiate.

An analysis of the distribution of angle β is presented in this section (Fig. 11). Angle β is the angle between the slip direction and the normal to the free surface (Fig. 11a). It can be linked to the height h of the step created on the surface by an elementary slip along the slip direction through the following equation:

$$h = \cos\beta \quad (1)$$

As above, 91 SB cracks initiated in 91 grains of the two zones were analyzed. The distribution of the angle between the slip direction and the normal to the surface (β) is plotted in Fig. 11b with respect to the Schmid factor of the slip system associated with the crack. As previously, grains have been divided into three groups, depending on the difference between the highest Schmid factor of the grain and the Schmid factor related to the cracked slip system. Almost no crack initiated in the domain $\beta \in [0°, 20°]$. A near-symmetrical triangular distribution can be observed, centered on the range [50°, 60°], which represents about 25% of the cracks initiated in PSBs. Over 66% of the cracks initiated with an angle β in the domain [40°, 70°]. These results are in good agreement with results of the literature obtained on isotropic specimens [26]. However, the texture of the material has also a great influence on the crack distribution, as shown by Mineur et al. [26]. The distribution of angle β associated to the cracks can be compared to that of β of the slip system having the highest Schmid factor in all the grains in the analyzed zone (Fig. 11b). It can be seen that the distributions have similar shapes, but with different levels. Cracks along slip systems having β in the range [40°, 70°] are over-represented compared to the global distribution, whereas cracks with angle β belonging to [0°, 20°] or [70°, 90°] are under-represented.

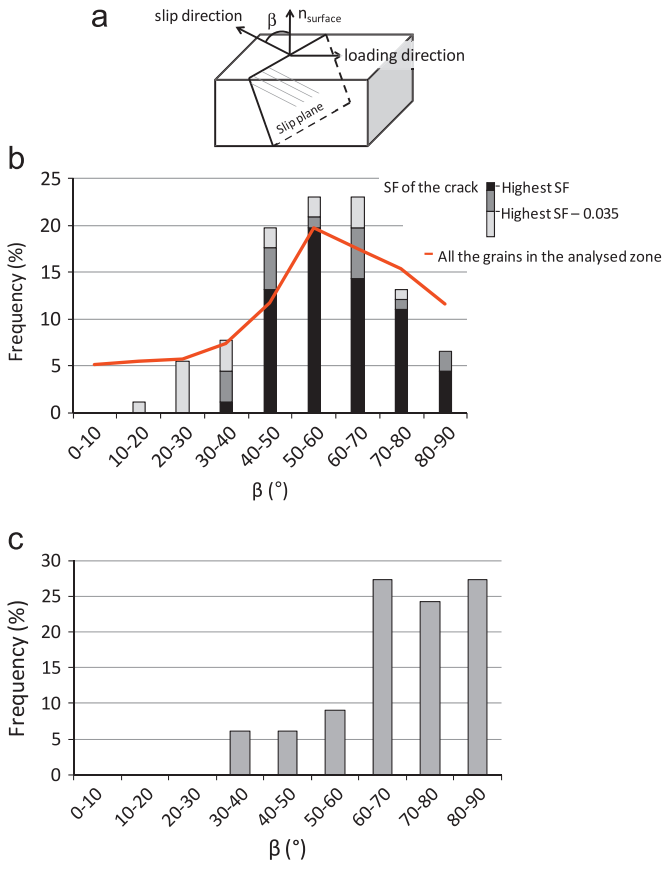

Fig. 11. (a) Angle between the slip direction and the normal to the surface, β (b) distribution of angles β of the slip systems associated with cracks with respect to the Schmid factor (for cracks initiated in slip bands) together with the angle made by the slip direction of the slip system having the highest SF in all the grains of the analyzed zone. Cracks are split into three groups depending on the value of the Schmid factor associated with the crack compared to the highest Schmid factor of the grain. (c) Distribution of β in grains showing cracks for the slip systems having the highest Schmid factor but not turned into cracks.

Cracks appeared in slip system not well oriented have been studied specifically. For the cracks with low Schmid factors (3rd group), the distribution of angle β is moved to the left in comparison with the distribution of β for grains well oriented (1st and 2nd groups). For the 3rd group of crack, angle β belongs to [10°, 70°]. In these grains, the orientation of the best oriented system has been analyzed. The distribution of angle β for the slip system having the highest Schmid factor in grains of the 3rd group is shown in Fig. 11c. In these grains, the slip systems having the highest Schmid factor have a slip direction mostly in the range [60°, 90°], which corresponds to slip systems having a small emerging volume (Fig. 12) and are also systems of type B [32]. Using dynamic dislocation simulations, Déprés proposed a criterion for crack initiation under biaxial cyclic loadings in slips system oriented for double glide and having the highest emerging volume [33]. Slip systems showing crack initiation in our case are not oriented for double glide, but the rule of the maximum emerging volume is still valid, as it can be seen in Fig. 11. Most of the slip systems badly oriented in the sense of the maximum emerging volume criterion do not lead to crack initiation, which occurs in a different slip system. There is then a selection of the slip system on which crack will appear depending on the slip direction. Under uniaxial loading, the rule of the maximum emerging volume is equivalent to the analysis proposed by Brown and Miller [32].

It is interesting to consider the effect of coupling angles β and Π on crack initiation. Fig. 13 shows the combined distribution of these two angles, on one hand, for the best oriented slip system in all the grains and, on the other hand, for slip systems associated with initiated PSB cracks. Values of β and Π of slip systems with the highest Schmid factor cover a large domain (Fig. 13a), highlighted by the white dotted bands. It is clear that cracks initiated

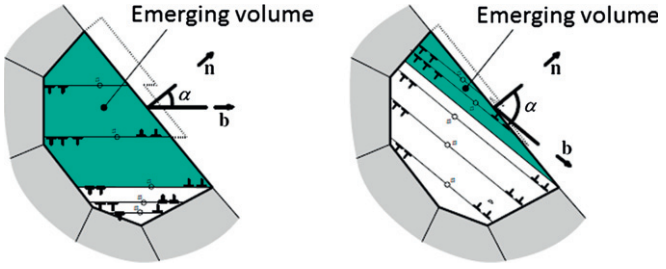

Fig. 12. Assumption of the maximum emerging volume [33].

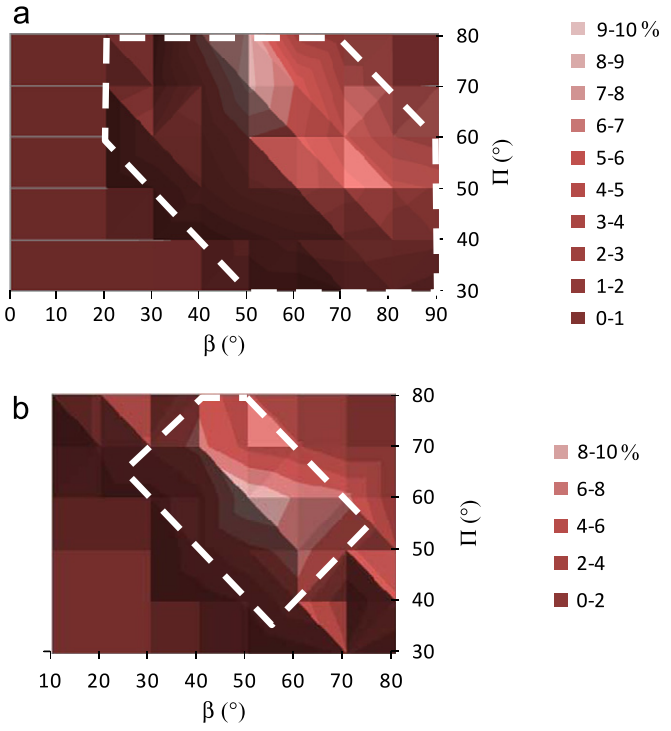

Fig. 13. Distribution of angles β and Π of (a) slip system with the highest Schmid factor and (b) initiated slip band cracks.

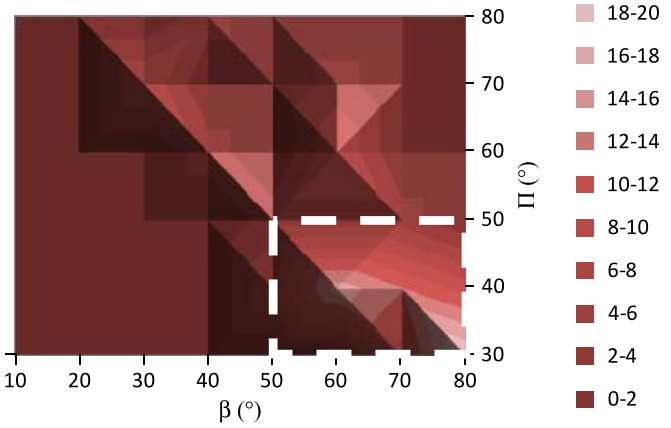

Fig. 14. Combination of angles β and Π of slip systems corresponding to the maximum Schmid factor but not turned into cracks in grains showing slip band cracks.

only in a smaller domain limited by the white dotted bands in Fig. 13b. The maximum is obtained when $\beta = 50^\circ$ and $\Pi = 70^\circ$. This figure clearly indicates a correlation between the values of β and Π for crack initiation. This correlation can be expressed by the following relations:

$$30^\circ < \beta < 60^\circ \tag{2}$$

$$\Pi = 110 - \beta \pm 20^\circ \tag{3}$$

It can be observed that in the lower right corner of the global domain, where β is maximum but Π minimum, only few cracks are initiated.

The distribution of the angles β and Π of slip systems corresponding to the maximum Schmid factor of the grain considered but not turned into cracks is also analyzed. As shown in Fig. 14, most favorably oriented slip systems with $\beta \in [50^\circ, 90^\circ]$ and $\Pi \in [30^\circ, 50^\circ]$ (zone limited by white dotted bands) did not turn into crack during the fatigue test. This corresponds to the domain showing few slip systems in the lower right corner in Fig. 13.

5. Conclusion and prospect

A tension–compression fatigue test was carried out; the surface of the specimen was observed during the test with an in situ microscope and after the test by SEM. Crystallographic orientations of the grains were obtained by EBSD after the mechanical test. It can be seen that the plastic activity appears very early during cycling, as over 75% of the slip markings appear before 500 cycles. The first various crack initiation sites were studied. 94% of cracks initiated in slip bands or at grain boundaries. Crack orientations were measured and analyzed; and the slip systems associated to cracks have been identified by comparing the measured crack orientations to the orientations of all potential slip systems. It was shown that about 2/3 of cracks make an angle with the loading axis in the range [50°, 80°] and that about 2/3 cracks initiate in slips systems with the highest Schmid factor. It was also found that if a slip band with the maximal Schmid factor in a given grain has an orientation of about 45° with respect to the load axis, which is the case of grain A in Miller classification [32], a crack may initiate in another slip system, especially if the angle between the slip direction and the normal to the surface is wide.

Acknowledgments

This work is part of a thesis financed by CSC (China Scholarship Council). The authors also wish to thank ECOS-Sud program, who financed the travel and stay in Argentina during the cooperation between Laboratoire de Mécanique de Lille (France) and Instituto de Física Rosario (Argentina). They would like to show their gratitude to Fernando Ugo (Instituto de Física Rosario, Argentina), who helped to realize the fatigue test and in situ observations in Argentina. The authors are also grateful to Colette Rey, Julien De Jaeger and Françoise Garnier (MSSMat, Ecole Centrale Paris) for the EBSD measurements.

References

[1] T. Obrtlík, Kruml, J. Polák, Mater. Sci. Eng. A 187 (1994) 1–9.
[2] T. Kruml, J. Polák, K. Obrtlík, S. Degallaix, Acta Mater. 45 (1997) 5145–5151.
[3] G. Kang, Y. Dong, H. Wang, Y. Liu, X. Cheng, Mater. Sci. Eng. A 527 (2010) 5952–5961.
[4] Y. Dong, G. Kang, Y. Liu, H. Wang, X. Cheng, Mater. Char. 65 (2012) 62–72.
[5] J. Man, P. Klapetek, O. Man, A. Weidner, K. Obrtlík, J. Polák, Philos Mag 89 (2009) 1337–1372.
[6] J. Polák, J. Man, T. Vystavěl, M. Petrenec, Mater. Sci. Eng. A 517 (2009) 204–211.
[7] J. Man, T. Vystavěl, A. Weidner, I. Kuběna, M. Petrenec, T. Kruml, J. Polák, Int. J. Fatigue 39 (2012) 44–53.
[8] M. Kamaya, Mater. Charact. 60 (2009) 1454–1462.
[9] C. Blochwitz, S. Jacob, W. Tirschler, Mater. Sci. Eng. A 496 (2008) 59–66.
[10] S. Degallaix, R. Taillard, J. Foct, Fatigue 84, in: C.J. Beevers (Ed.), vol. 1, pp. 49–59, 1984.
[11] S. Degallaix, A. Seddouki, G. Degallaix, T. Kruml, J. Polàk, Fatigue Fract. Eng. Mater. 18 (1995) 65–77.
[12] J.-B. Vogt., J. Mater, Process Technol. 117 (2001) 364–369.
[13] W.Y. Maeng, M.H. Kim, J. Nuclear Mater. 282 (2000) 32–39.
[14] U. Lindstedt, B. Karlsson, M. Nyström, Fatigue Fract. Eng. Mater. 21 (1998) 85–98.
[15] C. Zong, N.Y. Jin, X. Zhou, E. Meng, X.F. Chen, Acta Metall. Mater. 38 (1990) 2135–2140.
[16] A. Mateo, L. Llanes, L. Iturgoyen, M. Anglada, Acta Mater. 44 (1996) 1143–1153.
[17] S.E. Moussavi Toorshizi, Ph.D. Thesis, University of Lille 1, 1997.
[18] V. Aubin, Ph.D. Thesis, University of Lille 1, 2001.
[19] A. El Bartali, V. Aubin, S. Degallaix, Int. J. Fatigue 31 (2009) 2049–2055.
[20] A. El Bartali, V. Aubin, S. Degallaix, Adv. Eng. Mater. 11 (2009) 727–731.

[21] A.C. Marinelli, A. El Bartali, J. Signorelli, P. Evrard, V. Aubin, I. Alvarez-Armas, S. Degallaix-Moreuil, Mater. Sci. Eng. A 509 (2009) 81–88.
[22] X. Feaugas, C. Gaudin, Mater. Sci. Eng. A 309–310 (2001) 382–385.
[23] J. Schwartz, Ph.D. Thesis, Ecole Centrale Paris, 2011.
[24] B. Chang, Z. Zhang, Mater. Sci. Eng. A 556 (2012) 625–632.
[25] V. Gerold, H.P. Karnthaler, Acta Metall. 37 (1989) 2177–2183.
[26] M. Mineur, P. Villechaise, J. Mendez, Mater. Sci. Eng. A 286 (2000) 257–268.
[27] M. Mineur, Ph.D. Thesis, University of Poitiers, 2000.
[28] M. Kamaya, Fatigue Fract. Eng. Mater. 33 (2009) 94–104.
[29] H. Mughrabi, R. Wang, K. Differt, U. Essmann, Fatigue Mechanisms, ASTM STP 811, American Society for Testing and Materials, pp. 5–45, 1983.
[30] J.Y. Buffière, E. Ferrié, H. Proudhon, W. Ludwig, Mater. Sci. Technol. 22 (2006) 1019–1024.
[31] A. King, W. Ludwig, M. Herbig, J.Y. Buffière, A.A. Khan, N. Stevens, T.J. Marrow, Acta Mater. 59 (2011) 6761–6771.
[32] M.W. Brown, K.J. Miller, Proc. Inst. Mech. Eng. 187 (1973) 65–73.
[33] C. Déprés, Ph.D. Thesis, Institut National Polytechnique De Grenoble, 2004.